Heat source and voiding signatures of Mullins damage in filled EPDM

Nicolas Candau, Oguzhan Oguz, Edith Peuvrel-Disdier, Jean-Luc Bouvard, María Lluïsa Maspoch, Guillaume Corvec, Christophe Pradille, Noëlle Billon

Heat Source and Voiding Signatures of Mullins Damage in Filled EPDM

Nicolas Candau [1,], Oguzhan Oguz [2], Edith Peuvrel-Disdier [3], Jean-Luc Bouvard [3], María Lluïsa Maspoch [1], Guillaume Corvec [3], Christophe Pradille [4], Noëlle Billon [3]*

[1] Centre Català del Plàstic (CCP) - Universitat Politècnica de Catalunya Barcelona Tech (EEBE-UPC), Av. D'Eduard Maristany, 16, 08019, Spain

[2] Laboratory of Macromolecular and Organic Materials (LMOM), Institute of Materials (IMX), Ecole Polytechnique Fédérale de Lausanne (EPFL), Station 12, 1015 Lausanne, Switzerland

[3] Mines ParisTech, PSL Research University, CEMEF - Centre de Mise en Forme des Matériaux, UMR CNRS 7635, CS 10207, 06904 Sophia-Antipolis, France

[4] Mat-xper, 06560 Valbonne, France

[*]Corresponding author: nico.candau@gmail.com

Abstract

The thermomechanical coupling of Mullins damage in filled EPDM has been investigated by analysing the self-heating via Infrared thermography (IR) and the voiding fraction by Digital Image Correlation (DIC). The volumetric strain measured during the rubber deformation is found to be predominantly associated with damage, while thermal dilatation caused by self-heating has a negligible contribution. On this basis, the thermomechanical coupling of Mullins phenomena has been identified by evaluating the strain and time dependence of the following criteria: the tangent modulus, the voiding rate and the heat sources. The tangent modulus that reaches a maximum at the strain transition from a series of cycle to another is found to be an appropriate mechanical signature of Mullin softening. At the same strain transition, both voiding rate upturn and heat source upturn are observed. These signatures suggest the Mullins damage to be mainly associated at high strain rate with the (re)-activation of dissipative cavitation mechanisms, by nucleation of new cavities and/or acceleration of cavities growth.

Keywords

Rubber damage; self-heating; filled EPDM.

1. Introduction

Vulcanized rubber materials undergoing mechanical cycles exhibit significant change in their mechanical properties between the first loading and the following ones. This phenomenon is called Mullins' effect. In spite of a wide number of experimental and theoretical investigations on Mullins effect, only few of them focused on its mechanisms in extreme loading conditions such like those encountered in some industrial applications where rubber material undergoes high thermomechanical coupling, e.g. rubber deformation in pneumatic tire [1] or during the thermo-mechanical devulcanization [2].

Mullins effect is met in a wide number of rubber classes, namely Natural Rubber (NR) [3], Nitrile Butadiene Rubber (NBR) [4], Ethylene Propylene Diene Rubber (EPDM) [5], Polydimethylsiloxane (PDMS) [6], Styrene-Butadiene Rubber (SBR) [7], thermoplastic elastomers [8], [9] hydrogels [10], [11] and biological tissues [12]. These elastomeric materials generally exhibit multiple large strain mechanisms, such as viscoelasticity, inelasticity, crystallization and damage. Among these mechanisms, Mullins damage refers to the mechanisms involved in cyclic loading of filled rubber associated with chains rupture and/or debonding at filler interface. Damage is a mechanism associated with void creation which hence generates a raise of volumetric strain accessible by Digital Image Correlation (DIC) [13]. Like dilatometry [14], such technique provides access to the materials porosity [15]. It may be a convenient experimental means to isolate Mullins damage to other large strain mechanisms. DIC has been used to provide insight of damage at rubbery network chains scale, when combined with thermoporosimetry. Thermoporosimetry provides the distribution of voids size at chains network scale [16],[17]. It has been employed to observe rubber damage induced by irradiation, [18] ageing [19] or stretching [20] at chains length scale. More specifically, such methods, when combined with DIC, may

provide real time measures of network chains scale damage induced by the deformation [21],[22]. By quantifying volume fraction of the voids (DIC) and void size (SAXS) [23], it was concluded that Mullins damage may be accompanied by the progressive closing of cavities during unloading, and that the subsequent increase of the strain involves the nucleation/growth of new cavitation sites.

The above-mentioned studies focus on Mullins damage phenomena in quasi-static conditions, i.e. non-adiabatic conditions yielding to the absence of a measurable thermomechanical coupling, or they did not use experimental means to reveal the possible existing thermomechanical coupling.

However, thermomechanical coupling should be considered in polymer and rubber materials, especially concerning the investigation of high strain rate deformation mechanisms [24] or fatigue damage [25]. In polymers, heat-dissipation is a known signature used to detect the mechanical damage initiation. The latter indeed generates heat which can be measured as an overall increase of the specimen temperature [26]. Additionally, self-heating has been used to determine the fatigue limit of polymers by estimating the critical fatigue damage. This has been performed by applying progressive loads. The temperature increased until it stabilizes for each applied stress level, and the stabilized temperature then provides an estimate of the damage [27].

Thermomechanical coupling should also be considered in rubber materials that undergo damage in high strain rate loading conditions, hence possibly involving high thermal dissipation. This is also crucial in industrial rubbers containing highly dissipative carbon black fillers. As an example, a self-heating of 25 °C above RT (room temperature) may be induced by large cyclic loading (200%) at high frequency (40 Hz) of filled rubber specimen (conditions possibly met in a pneumatic tire at a crack zone) may cause the premature melting of reinforcing strain induced crystals of NR[28]. This temperature can reach +60 °C above RT in rubber into a pneumatic tire

under fatigue condition [1]. In thermo-mechanical devulcanization process, the high shear deformation applied to the rubber results in self-heating of 55 °C above RT [2] and then may participate to the rubber degradation.

As a result, many mechanisms may occur concomitantly in cyclically deformed filled rubber, such as strain induced crystallization, viscoelasticity and damage that all dissipate energy into heat in adiabatic conditions (high deformation rate). They are consequently difficult to identify separately. Considering that part of mechanical dissipation in highly deformed rubber originates from damage, and is further converted into heat [29], Le Cam et al. showed that damage in filled rubbers can be distinguished from other dissipative contributions [30]. This has been possible by performing an analysis of the thermal sources based on Infrared thermography proposed to discriminate the diverse contribution of Mullins effect (viscoelasticity, thermoelasticity, damage) [31].

Infrared thermography (IR) and Digital Image Correlation (DIC) have been coupled to give insights on thermomechanical behaviour of polymeric systems [32], [33], [34]. However, their combination to identify the relationship between the thermal response of dissipative mechanisms and the possible associated volumetric strain (damage) response has rarely been discussed yet. In particular, there is no study in the literature that already combined thermal and strain fields to investigate Mullins damage in adiabatic conditions. The development of an *ad-hoc* experimental method that is able to account for such thermal dissipation depending on the level of cavitation, is still missing.

This study proposes the first investigation on the thermomechanical coupling of the Mullins damage in filled rubber by combining the analysis of voiding signature by Digital Image Correlation (DIC) and of the heat source signature by Infrared thermography (IR). In a first section we present the theoretical frame used to identify the heat sources generated during cyclic tests. In

a second section, we account for potential effect of thermal dilatation that may perturb the measure of the volumetric strain generated by the rubber deformation. In a third section, we present the combined self-heating and volumetric strain responses during cyclic test in filled EPDM containing 0, 40 and 80 phr (per hundred rubber) of carbon black. The damage experienced during mechanical cycles generates (i) an increased volumetric strain due to voiding and (ii) a self-heating due to dissipated mechanical energy and thermoelastic coupling. In a fourth section, the thermomechanical coupling of Mullins damage has been evaluated by analysing the voiding rate and the heat sources. At the strain transition from a series of cycle to another by incremental strain (Mullins type test), we show simultaneous voiding rate upturn and heat source upturn, demonstrating the Mullins damage to be essentially associated with the (re-)-activation of dissipative cavitation mechanisms.

2. Materials and methods

2.1. Materials composition and processing

The materials provided by the SACRED Group are extended oil carbon black filled EPDM (Keltan 5470) obtained by sulphur vulcanization of the gum. They contain 70% in mass of Ethylene and 4.6% of ethylidene norbornene (ENB). All materials contain 0, 40 or 80 phr (phr means per 100 g of rubber) of carbon black (N550); They all contain 4 phr of calcium oxide, 5 phr of zinc oxide, 1 phr of stearin, 2 phr of Polyethylene Glycol (PEG 4000) as plasticizer. The vulcanization components are 1.2phr of sulfur (75%), 1 phr of mercaptobenzothiazole (MBT 75%), 0.8% phr of mercaptobenzothiazole disulfide (MBTS 75%), 1.2 phr of N-cyclohexyl-2-benzothiazolesulfenamide (CBS 75%) and 1.5 phr of zinc dialkyl dithiophosphate (ZDTP 70%). An internal mixer (Brabender®) is used for the rubber compounding. Sample sheets are produced by curing in a hot press at 170°C for with a curing time $t_{100\%}$ =15 minutes, a time corresponding to

the moment when the torque reaches 100% of maximum RPA using a Moving Die Rheometer MDR (D-RPA 3000, Montech). Dumbbell-shaped samples, with a 15 mm gauge length (L_0), 6 mm thickness and 10 mm width, are then prepared for tensile testing.

2.2. Thermal dilatation due to external heating measured by Digital Image Correlation (DIC)

The thermal dilatation due to external heating on unstretched rubber (no external tensile forces) is measured by DIC (VIC-3D software package) performed on the front and side surfaces of the specimen. To obtain consistency with further measures of volumetric strain during tensile tests (see section 2.3), the specimens are gotten from the central part of unstretched dogbone-shaped specimen similar to those used for mechanical tests. The specimen are put into an oven and subjected to heating at 10°K per minute by steps of 5°K where series of five DIC images are recorded. The coefficient of thermal expansion at constant pressure (no external stress is applied to the specimen except atmosphere pressure) induced by external heating is provided by the measure of the slope of the volumetric strain versus the specimen temperature as given by:

$$\alpha = \frac{1}{v}\frac{dv}{dT} \tag{1}$$

Volumetric strain has been measured during heating from external source and cooling down to room temperature in absence of any external tensile forces (unstretched rubber) (**Figure 1a-b**). The strain fields on front and side surfaces are determined from a region of interest (ROI) on each face. Hence, the principal strain λ_1, λ_2 and λ_3 are measured directly. The compared evolution of volumetric strain during heating and cooling (**Figure 1c**) shows good superimposition of temperature dependence suggesting no glass or phase transition in the temperature range studied.

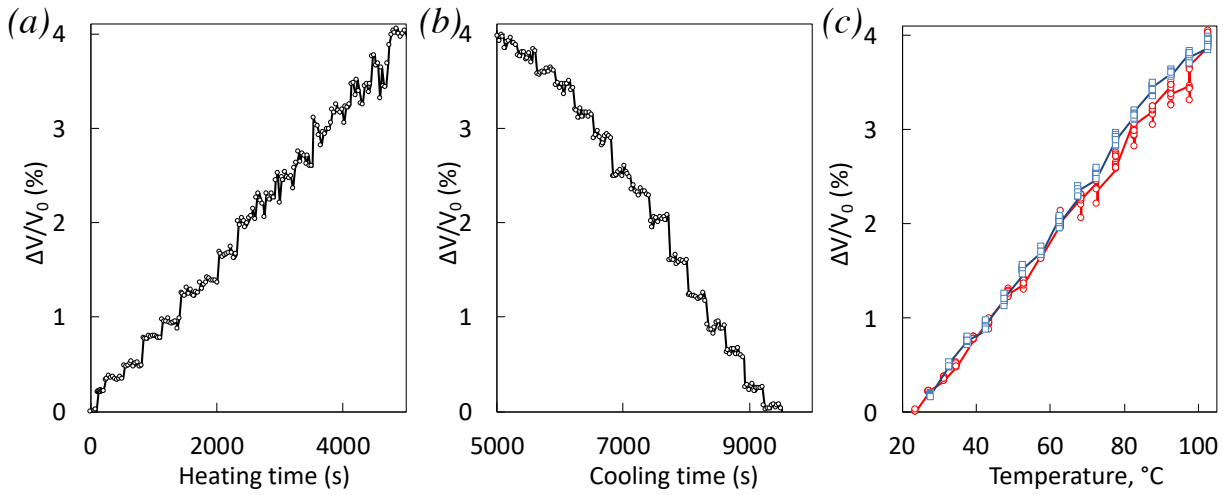

Figure 1. Volumetric dilatation (in %) due to external heating measured by DIC performed on front and side surfaces of the rubber specimen during heating/cooling at 10K.min^{-1}. Volumetric dilatation has been measured during heating *(a)* and cooling *(b)* as a function of the time. The comparative evolution of volumetric strain during cooling/heating is presented in figure *(c)*.

2.3. Thermomechanical set-up by Infrared Spectroscopy (IR) and Digital Image Correlation (DIC)

An electromechanical tensile test machine (INSTRON 5960 Series Universal Testing Systems) is used to perform mechanical tests (both loading and unloading) at room temperature (**Figure 2**). The nominal tensile strain rate of 1s^{-1} (15 mm.s^{-1}) is applied for these tests. Front and side surfaces of the samples are coated with a white spray paint in order to generate a random speckle pattern whose displacement will be further analysed by a VIC-3D software package. A four-cameras setup consisting of two-pairs systems is used to record the displacement fields on both front and side faces of the sample (**Figure 2a**). Two of them are AVT PIKE 5 Megapixels, with a 2/3' CCD sensors (front face camera system) and the other ones are AVT PIKE 4 Megapixels, with CCD sensors size equal to 1' (side face camera system). Both systems are respectively mounted with 25mm and 50mm Schneider Kreuzwach objectives. The experimental set-up has been fully described in a previous work [35], and the main steps are reported here. The post-processing of a series of images recorded is performed using VIC-3D software package. 3D DIC displacement

data are converted into strain values (**Figure 2b,d**). λ_1 represents the stretching ratio in the tensile direction, whereas λ_2 and λ_3 correspond to the transversal stretching ratios in the directions of the sample width and thickness, respectively. the transversal and longitudinal strains are homogeneous in the center of the sample and significantly decrease close to the clamping zones. The strain fields in both front and side surfaces are determined from a region of interest (ROI) in the central part of the sample. The ROI is meshed by using the VIC-3D software package, allowing tracking the speckle pattern during the tensile test. The ROI is chosen around 100 pixels for the front face and 60 pixels for the side face.

Details on the choice of DIC parameters can be found in reference [35]. The true stress is defined as the ratio between the applied force F and the specimen cross-section:

$$\sigma_T = \frac{F}{L_0 e_0 \lambda_2 \lambda_3} \tag{2}$$

where L_0 =15mm is the initial length and e_0 =4mm the initial width. The volumetric strain $\Delta V/V_0$ is defined as:

$$\Delta V/V_0(\lambda) = \lambda_1 \lambda_2 \lambda_3 - 1 \tag{3}$$

Rubber samples are stretched at different maximum strains. As seen in **Figure 2d**, the transverse and longitudinal strains are homogeneous in the center of the sample and significantly decrease close to the clamping zones. The strain field in both front and side faces are obtained in the central part of the sample. Trace of self-heating generated in the sample is recorded on its surface during the deformation using FLIR SC5000 camera (**Figure 2c**). Temperature field is analysed on the front face of the specimen with ALTAIR software [36] in the same ROI than for DIC analysis.

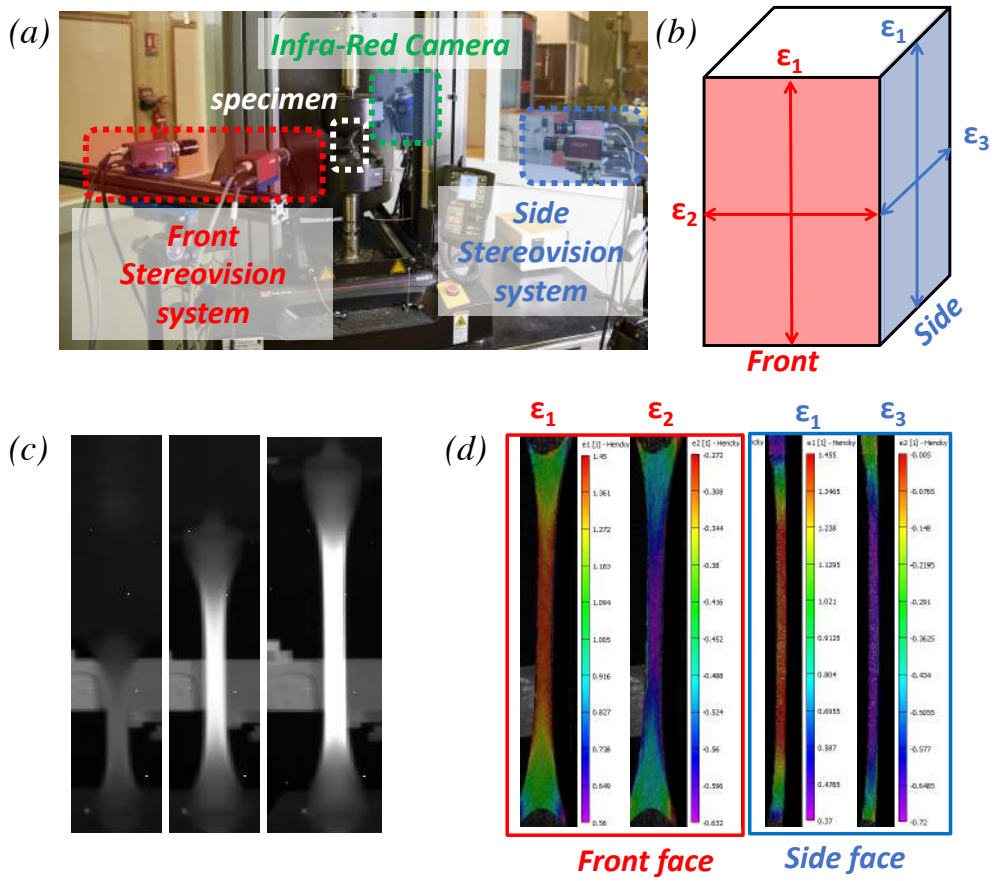

Figure 2. *(a)* Experimental Digital Image Correlation (DIC) set-up based on two independent stereo-vision systems to measure simultaneously strain fields on front and side surfaces of specimen, *(b)* Schematic representation of the front and side faces of the specimen with directions of the principal strain ε_1 on front and side face, ε_2 on front face and ε_3 on side face. ε_1 is calculated as the average value obtained on front and side surfaces, *(c)* traces of self-heating (in white) measured on the specimen surface at various deformation, *(d)* longitudinal and transverse strain fields analysed on front and side faces of the specimen for a given macroscopic deformation.

3. Results and discussion

3.1. Heat sources

In absence of phase transition, thermomechanical coupling describes elastic (entropic elasticity) and inelastic (damage, viscoelastic) deformation processes. The integration of elastic mechanisms to time over one cycle is zero. Assuming that for uniaxial tests, the heat source distributions are

uniform during the test, within the specimen surface (linearization of heat losses), the heat equation can be written [37],[30]:

$$\rho C\left(\dot{\theta}+\frac{\theta}{\tau}\right)=S \tag{4}$$

with ρ is the bulk density (g.cm^{-3}) of the EPDM materials, C its heat capacity (J.g^{-1}°C^{-1}), θ the temperature variation above the room temperature, $\dot{\theta}$ the rate of heating (W.m^{-3}) and S the heat source. For sake of simplicity, as proposed in Ref. [38], a normalized heat source s will be defined in the following as the ratio $s=S/\rho C$ and expressed in °C.s^{-1} . All designated as "heat source" in the following will refer to the quantity s. The time constant τ (s) characteristic of the heat loss along the specimen thickness is given by:

$$\tau=\frac{\rho Ce}{2h} \tag{5}$$

e is the thickness of the specimen and h the convection coefficient. In order to determine the constant time, the specimen was rapidly stretched at room temperature and at 1.s^{-1} up to failure. Due to energy dissipation induced by the specimen deformation, the material undergoes self-heating. The temperature measurement by IR thermography was then performed on the surface of self-heated broken (and relaxed) specimen during the return to room temperature. Exponential law was applied to determine the time constant τ_0 for relaxed specimen with the thickness e_0 (thickness of undeformed specimen) :

$$\theta=\theta_0 e^{-}\frac{t}{\tau} \tag{6}$$

This law was used to fit the temperature on the specimen surface during cooling down to room temperature (**Figure 3**). One can note that such law is not universally used to quantify the return

to room temperature of heated materials and is expected to widely depend on the heating conditions (self-heating, external heating), nature of the material and temperature measurement tool. Cooling temperature versus time of a composite polymer after external heat excitation may follow logarithmic law [39], inverse square root law [40]. However, same law was proposed to fit the temperature decrease down to room temperature of SBR [3],[30] and NR [38] rubber specimens heated by contact with a hot piece for a few seconds. By applying such exponential low in the present study, the constant time estimated for the relaxed specimen with the thickness e_0 was found equal to 27 seconds. The dependence of this time constant to the applied deformation was then identified using equation 5 and assuming a thickness reduction with longitudinal deformation, $e = e_0/\sqrt{\lambda_1}$. Hence the constant time is proposed to depend on the deformation as follows: $\tau = \tau_0/\sqrt{\lambda_1}$. Such approach permits to deduce constant times depending on the applied strain in the range of those obtained by Samaca Martinez et al. [3],[30],[38].

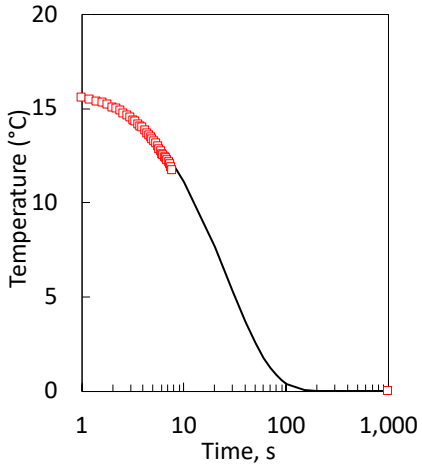

Figure 3. Temperature versus time after rapid loading at $1.s^{-1}$ and rupture of the rubber specimen. The fitting law is an exponential function whose characteristic time is used to define the diffusion time on the rubber specimen surface.

3.2. Volumetric strain induced by thermal dilatation

Severe loading conditions are accompanied by wide thermomechanical coupling. Hence, prior to the characterization of strain induced damage (section 3.3), it is necessary to evaluate the effect of the thermal dilatation on the volumetric strain response. Thermal dilatation potentially induced by self-heating of the filled rubber during cyclic loading may indeed generate a supplementary volumetric expansion that yield into a biased estimate of the damage (voids). The thermal expansion (volumetric expansion due to heating of the rubber specimen without any external stress) has been studied in a large temperature range well above the glass transition, from room temperature to 100 °C, (**Figure 1**), largely covering potential self-heating of the rubber specimen in cyclic loading conditions (see section 3.3).

For all series of filled EPDM, the volume expansion due to external heating and without external stress is found to increase linearly from room temperature to 100 °C (**Figure 4a**). This trend is consistent with the absence of phase transition or glass transition, due to the amorphous and rubbery nature of the series of EPDM in this temperature range. Such observation confirms the absence of hysteresis in the thermal dilatation behaviour between cooling and heating (**Figure 1c**). The slope of volumetric expansion with temperature decreases with the filler content (from 0 to 80 phr). The thermal expansion coefficient of the rubber specimen (considered as a composite of rubber and carbon black filler) extracted from this slope is found to decrease from 6.3 to 5.1×10^{-4}/°C by increasing the filler content (**Figure 4b**). Such trend is expected owing the lower thermal expansion of carbon black particles as compared to rubber phase [41]. While the thermal expansion coefficients are found to be independent of filler size, they significantly depend on the volume fraction of filler [42]. Contrarily to what can be expected from simple rule of mixture (linear dependence of expansion coefficient with carbon black volume fraction), no additivity of the thermal dilatation of the rubber phase and fillers is observed. Instead, the thermal coefficient

expansion rapidly decreases from EPDM-0 to EPDM-20 (10 vol.%) but then stabilizes for higher filler contents. This is consistent with the presence of a 3D filler network in all filled EPDM (from EPDM-20 to EPDM-80) as shown by their high electrical conductivity [43], so that the immobilized rubber phase in the filler vicinity (occluded and bonded rubber) may play an important role in the restriction of thermal expansion. Due to reaggregation of such filler network upon loading [44], it will be assumed that the thermal dilatation induced by temperature changes (e.g. due to strain induced self-heating) during mechanical loading (cf. section 3.3) is expected not to significantly change with the level of deformation of the specimen.

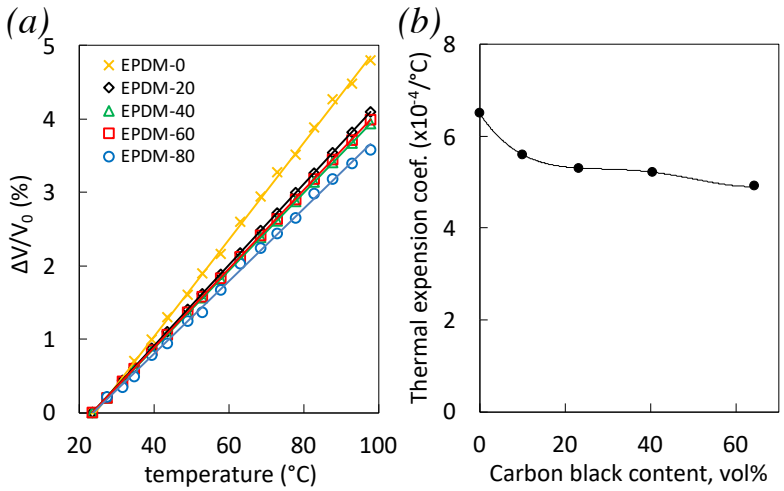

Figure 4. *(a)* Volumetric deformation due to thermal dilatation measured by DIC performed on surface of the rubber specimen, *(b)* Thermal expansion coefficients deduced from figure 4a for a series of EPDM with various carbon black contents from 0 to 80 phr (per hundred rubber).

3.3. Thermal and volumetric strain signatures of Mullins damage

Mullins effect is a softening mechanism characterized by a stress decrease during unloading as compare to the stress during loading at the same strain [45]. Additionally, significant stress drop between successive loading, especially between the first and second cycles, is characteristic of the Mullins effect. This drop becomes negligible after 5-10 cycles. The relationship between the mechanical behaviour, volumetric strain and thermal behaviour is studied here to further propose

a full thermomechanical description of damage mechanisms associated with Mullins effect. Assuming that external heating (see previous section) and strain induced self-heating cause similar volumetric expansion, the contribution of the volumetric strain induced by the self-heating during the loading can be identified separately to the overall volumetric strain (including both strain induced damage and thermal expansion). Such equivalence between external heating and self-heating also assumes the difference of temperature profiles in the thickness for the two types of heating to be not drastically different. First, the slow external heating of undeformed specimen to identify thermal dilatation (**Figure 4**) is expected to be uniform with thickness (linear profile within the thickness). Second, the temperature field measured on the specimen surface during the tensile tests is assumed to be representative of the mean distribution of temperature field in the thickness of the specimen.

To evaluate the coupling between damage (DIC) and self-heating (IR) under cyclic conditions, the specimens have experienced incremental cyclic loading (**Figures 5-7**) at a nominal strain rate of $1.s^{-1}$: 5 cycles with loading up to a fixed strain and unloading down to zero stress, successively up to λ_1, λ_2 λ_3 and λ_4. λ_1, λ_2 λ_3 correspond to maximum displacement of 30 mm, 60 mm and 90 mm respectively and λ_4 corresponds to strain to fail. The series of cycles performed up to λ_1, λ_2 λ_3 then roughly correspond to a frequency of cycles of 0.25 Hz, 0.125 Hz and 0.08 Hz assuming zero stress close to zero strain. This procedure is performed up to the failure of the specimen. As a reference material, the unfilled EPDM-0 (**Figure 5**) has experienced the same loading paths than the filled EPDM-40 (**Figure 6**) and EPDM-80 (**Figure 7**) studied hereafter. Moreover, for each material that undergoes cyclic test, a reference single loading test up to failure and at same strain rate has been performed (dotted line in **Figure 5d-f**, **Figure 6d-f**, **Figure 7d-f**). The two filled EPDM have been selected from the previous series of EPDM (**Figure 4**) as they belong to two different regimes of

damage mechanisms [43]. Indeed, a filler ratio transition in damage mechanisms had been identified in such materials, suggesting (i) damage to be predominantly localized in the rubber chains network in weakly filled EPDM ($\varphi \leq 40$ phr) and (ii) a strain transition from rubber chains network damage to filler network damage to occur in highly filled EPDM ($\varphi > 40$ phr). In the following, the two cases are studied by selecting the EPDM-40 and the EPDM-80 with filler content below and above the critical ratio respectively.

The case of unfilled EPDM-0 is first investigated. Softening associated with Mullins effect may be expected in unfilled rubbers [46]. As demonstrated by Mullins, the phase change (crystallization/melting) of the natural rubber (NR) upon deformation is responsible for such behaviour. In our unfilled EPDM-0, a non-crystallizing rubber, only minor stress softening due to cyclic accumulation is observed (**Figure 5a**). At the end of each series of cycles, when λ surpasses $\lambda_{max}=\lambda_1, \lambda_2, \lambda_3$ or λ_4 respectively the stress tends to follow the single tensile test curve (**Figure 5d**). The volumetric strain of the unfilled EPDM-0 shows decrease with cycles accumulation (except for the first series of cycles up to $\lambda_{max}=\lambda_1$) (**Figure 5b**) but does not show peculiar dependence on strain (**Figure 5e**). One may note that the volumetric strain due to thermal dilatation induced by self-heating (estimated from thermal expansion coefficient calculated in section 3.1 assuming equivalence between external heating source and self-heating source) has non-negligible contribution to the overall volumetric strain (cf. **Figure 5b**) but remains too low to obstruct the measure of DIC damage. The self-heating increases with time, but the effect of cycles accumulation is no more perceptible yet at the third series of cycles (**Figure 5c**). Regarding the strain dependence of self-heating, only weak hysteresis loops are observed (**Figure 5f**) and the temperature is only slightly higher than the one measured in single loading test suggesting heat

generation at surface of unfilled EPDM-0 to be mostly associated with reversible entropic coupling while only weak energy dissipation associated with damage and/or viscoelasticity takes place.

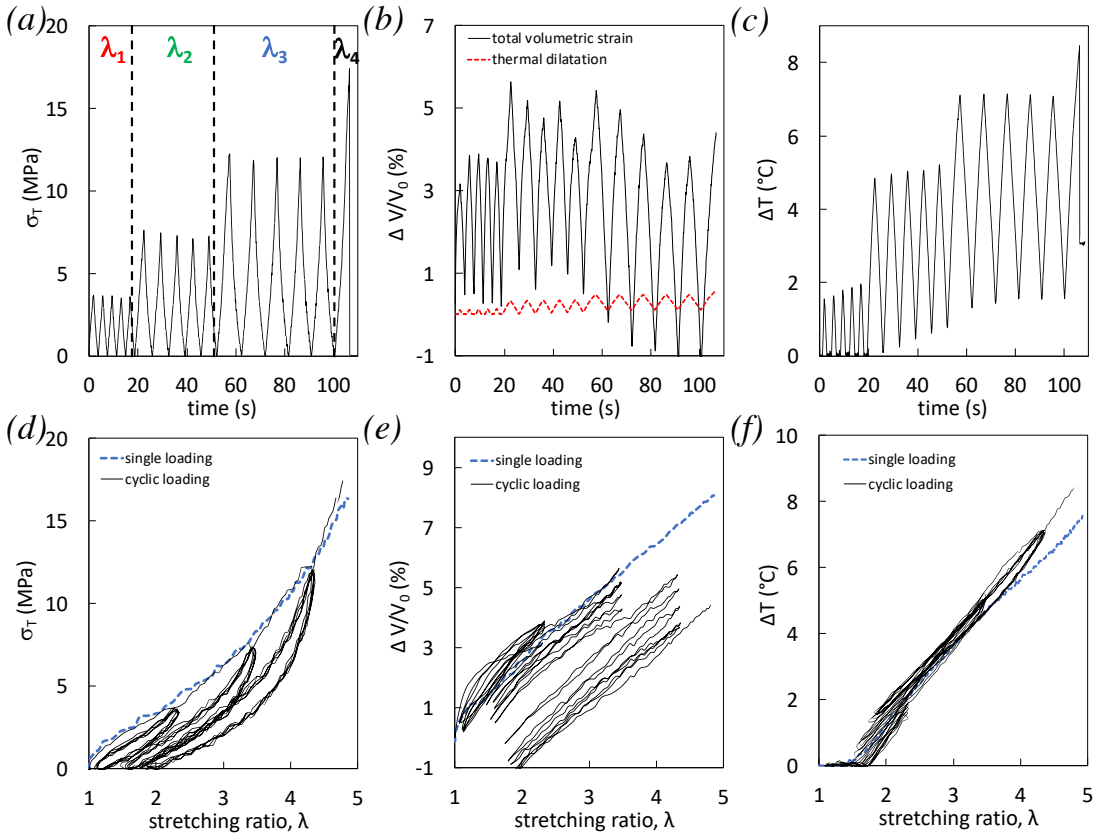

Figure 5. True stress *(a)*, volumetric strain *(b)*, self-heating *(c)* versus experimental time. Stress vs. strain *(d)*, volumetric strain vs. strain *(e)* and self-heating vs strain *(f)* for EPDM-0 during multiple uniaxial loading at the nominal tensile strain rate $1.s^{-1}$. The successive imposed strain are λ_1, λ_2 ,λ_3 and λ_4 but specimen undergo failure before reaching λ_4. Dotted line in figure *(b)* represents the expected volumetric strain originated by thermal dilatation estimated from figure 3 that may be ascribed to self-heating. Blue dotted line in figures d-f represent the reference single loading.

Contrarily to unfilled EPDM-0, the filled EPDM-40 exhibits stress softening by cyclic accumulation, especially for the highest applied cyclic strain λ_3 (**Figure 6a**), a typical feature of Mullins effect [45]. EPDM-40 does not show remarkable change in volumetric strain with cyclic accumulation except a slight increase for the highest applied cyclic strain λ_3 (**Figure 6b**) suggesting that voids closing is not favored by cyclic accommodation. This is confirmed by an observed higher volumetric strain at the end of the cyclic test as compared to one measured in

single test (**Figure 6e**). Like in EPDM-0, (**Figure 5c)** the maximum heat stabilizes at third series of cycles at $\lambda_{max} = \lambda_3$ (**Figure 6c**), but the absolute self-heating value is found to be higher. This is likely due to high viscous dissipation in presence of filler that may be due to frictional energy dissipation during interfacial sliding at the filler–filler and filler–rubber interfaces [47],[48]. Other dissipative damage may also take place at filler-rubber interface, like rubber chains rupture, and participate to the temperature rise. Nonetheless, assuming equivalence between self-heating and external heating on the thermal dilatation of the material, the thermal dilatation due to self-heating calculated from thermal expansion coefficient (section 3.2) has negligible contribution to the total measured volumetric strain (**Figure 6b**). The latter is thus expected to be representative of damage (voiding) induced by the specimen deformation. The first cycles for each $\lambda_{max}=\lambda_1$, λ_2, or λ_3 in EPDM-40 show large mechanical hysteresis that decreases and stabilizes for the subsequent cycles at the three λ_{max} (**Figure 6d**). As expected from Mullins effect, when λ surpasses λ_{max} the cyclic tensile curve joins the single tensile curve (**Figure 6d**). Contrarily to unfilled EPDM-0, the accumulation of heat on the specimen surface (**Figure 6f**) traduces disbalance between heating/cooling during cycles (see detailed study in section 3.4) that may arise from the accumulation of dissipative damage/viscoelasticity.

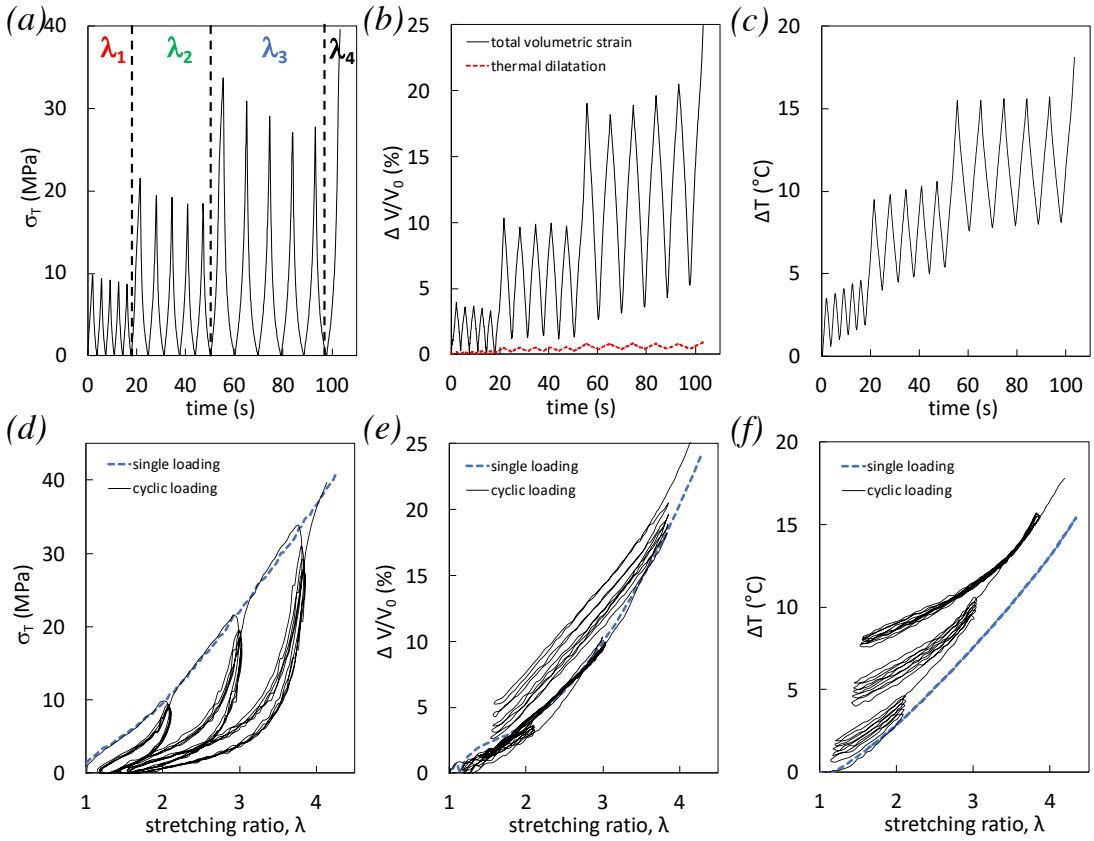

Figure 6. True stress *(a)*, volumetric strain *(b)*, self-heating *(c)* versus experimental time. Stress vs. strain *(d)*, volumetric strain vs. strain *(e)* and self-heating vs strain *(f)* for EPDM-40 during multiple uniaxial loading at the nominal tensile strain rate $1.s^{-1}$. The successive imposed strain are λ_1, λ_2, λ_3 and λ_4 but specimen undergo failure before reaching λ_4. Dotted line in figure *(b)* represents the expected volumetric strain originated by thermal dilatation estimated from figure 3 that may be ascribed to self-heating. Blue dotted line in figures d-f represent the reference single loading.

In EPDM-80, the stress at the various $\lambda_{max}=\lambda_1$, λ_2 or λ_3 decreases with cycles accumulation reflecting Mullins softening (**Figure 7a**). Similar to the stress response, the volumetric strain shows strong decrease with cyclic accumulation (**Figure 7b**). Like for EPDM 0 and EPDM 40, self-heating in EPDM 80 stabilizes at the third series of cycles (**Figure 7c**). In spite of the high self-heating with high filler content (**Figure 7c**), the contribution of thermal dilatation to the overall volumetric strain response of the highly filled EPDM-80 remains negligible (**Figure 7b**) due to low thermal expansion coefficient (**Figure 4b**) and conversely due to high expected strain induced void fraction in such highly filled material.

The resistance to failure in cyclic test is improved as compared to single test (**Figure 7d**). This may be explained by a delayed volumetric strain due to cyclic accumulation as compared to reference single test (**Figure 7e**), confirming a certain ability to accommodate damage in cyclic conditions. Additionally, one may note that the difference in self-heating between single and cyclic test exceeds 10 °C (**Figure 7f**). It has been shown that a reduction of the local confinement of the rubber in the filler vicinity with increased temperature yields in a delayed cavitation [49]. Hence, in addition to the materials ability to accommodate the cyclic accumulation at such high filler content that subsequently prevents the re-opening of cavities (**Figure 7e**), the increased temperature may also participate in delaying the void nucleation/growth yielding in increased strain at failure.

The thermal responses of cyclically stretched filled EPDM indicate dissipative mechanisms that should be put in perspective with voiding mechanisms. In the following section, the signature of heat sources ascribed to dissipative mechanisms is compared with the materials mechanical reinforcement and with the rate of voiding in order to identify the thermomechanical coupling of Mullins damage, namely the damage occurring during the first loading of a series of cycles.

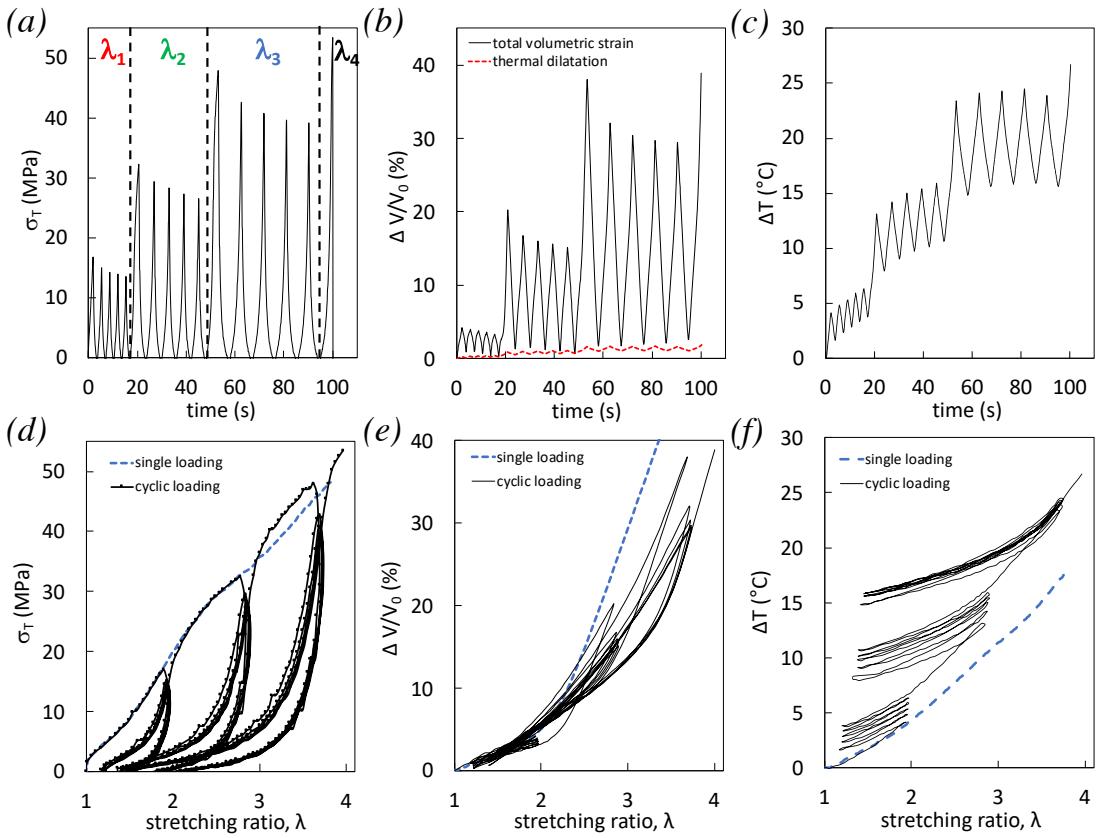

Figure 7. True stress *(a)*, volumetric strain *(b)*, self-heating *(c)* versus experimental time. Stress vs. strain *(d)*, volumetric strain vs. strain *(e)* and self-heating vs strain *(f)* for EPDM-80 during multiple uniaxial loading at the nominal tensile strain rate 1.s^{-1}. The successive imposed strain are λ_1, λ_2 ,λ_3 and λ_4 but specimen undergo failure before reaching λ_4. Dotted line in figure *(b)* represents the expected volumetric strain originated by thermal dilatation estimated from figure 3 that may be ascribed to self-heating. Blue dotted line in figures d-f represent the reference single loading.

3.4. Heat sources and voiding rate associated with Mullins damage

In order to investigate the thermomechanical coupling of Mullins damage, the following parameters are evaluated. First, the tangent modulus, estimated as the derivative of the stress versus strain, provides an information on the strain dependence of the materials reinforcement. Second, the rate of volumetric strain is defined as the speed of voids formation into the materials upon loading. Time and strain dependence of volumetric strain should be decoupled. In the strain range studied, the volumetric strain highly depends on the applied deformation but much less on time as identified during stress relaxation test as shown in figure 8 of Ref. [35]. Hence, the rate of

volumetric strain has been defined as the derivative of the volumetric strain as a function of the strain. Third, the heat source s, estimated in section 3.1 as the ratio $s=S/\rho C$ with S defined in equation 4, provides the strain and time dependence of heat exchanges between the specimen subjected to dissipative mechanisms (damage, viscoelasticity) and the environment.

EPDM-0 is first studied (**Figure 8**). No stress softening due to cycles accumulation is observed for cycles at λ_2 and λ_3 (**Figure 8a-b**). For the highest applied cyclic strain (λ_3), slight stress softening in unfilled EPDM-0 occurs between first and following cycles (2^{nd} to 5^{th}), that suggests slight accommodation mechanism (**Figure 8c**). The heat source is generated at a strain around 1.6 (**Figure 8i**). It is found to reach a positive value (heat dissipated by the material) around 2 °C/s during the diverse cyclic loadings and seen to slightly decrease down to 1.5 °C/s for the highest strain (**Figure 8i-l**). The heat source is nearly symmetric as same slope with negative values (heat absorbed by the material) are noted during unloading phases, and no effect of cyclic loading is observed.

The slight stress softening in unfilled EPDM-0 observed for the applied cyclic strain at λ_3 is not associated with peculiar signature in terms of heat source (**Figure 8k**) nor voiding rate (**Figure 8g**). Moreover, strain induced crystallization as a cause of such mechanism is not expected as it should have conducted to a typical exothermic signature [38]. One possibility is that such phenomena may be related to local damage at the interface between the rubber matrix and clusters formed from unreacted vulcanization components. Indeed, voids in the vicinity of ZnO clusters have been shown by SEM images in a previous work [21]. Such damage may occur with mechanisms similar to those of Mullins effect but at cluster interface instead of filler interface, via rubber chains slippage or breakage of bonded chains. Such damage is accompanied by lower level of heat dissipation – likely not perceptible on heat source (**Figure 8k**) – than expected in presence

of carbon black particles. Consistently, it is associated with no dramatic increase of voiding rate in the full range of strain studied (**Figure 8g**).

Filled EPDM samples are now investigated. Tangent modulus measured in both EPDM-40 and EPDM-80 measured during the first loading of the series of cycles with $\lambda_{max}=\lambda_2$, λ_3 and λ_4 (**Figure 9b-d**, **Figure 10b-d**) widely increases with strain up to a maximum (this corresponds to the strain where stress of cyclic test joins the one of the single curve) and then decreases. Tangent moduli of all following cycles (from 2nd to 5th) indicate a delay in reinforcement effect as compared to first cycles. For both EPDM-40 and EPDM-80, this suggests that most of the dissipative damage has occurred during the first cycle. Interestingly, during the first loading of each series of cycle with $\lambda_{max}=\lambda_2$, λ_3 and λ_4, the voiding rate is rather stable with strain but then suddenly increases at a strain corresponding to the strain at maximum tangent modulus, i.e. when the material is deformed above previous series of cycles (**Figure 9f-h**, **Figure 10f-h**).

It has previously been demonstrated in SBR and NR filled rubber that Mullins damage occurring during the first cycle yield in a deep increase of heat source [3]. This is consistent with our results obtained in EPDM as shown in **Figure 9j-l**, **Figure 10j-l**. Interestingly, this heat source is concomitant with the maximum tangent modulus and with the voiding rate upturn. For the subsequent cycles (from 2nd to 5th), a slight upturn of heat source is observed for the highest cyclic strain up to $\lambda_{max}= \lambda_3$ (**Figure 9k, Figure 10k**). Contrarily to Mullins damage seen in first cycle, this heat source signature is concomitant with the upturn of voiding rate with strain (**Figure 9g** and **Figure 10g**). Moreover, it shows more symmetry over the loading and unloading phases, consistent with weaker mechanical hysteresis observed for 2nd to 5th cycles (**Figure 6d** and **Figure 7d**).

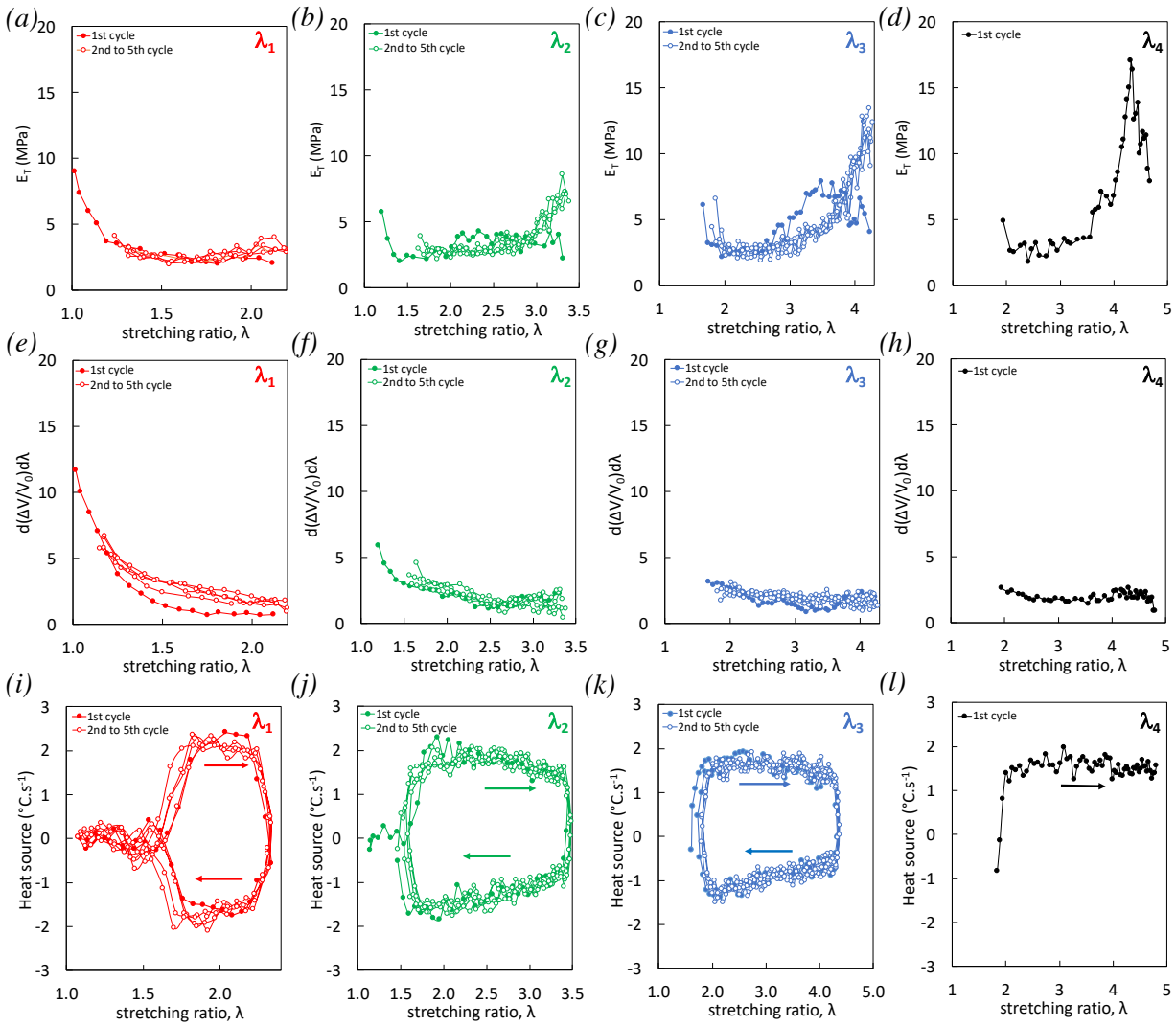

Figure 8. Tangent modulus *(a-d)*, voiding rate *(e-h)* and heat source *(i-l)* of EPDM-0 versus the different successive maximum strain (5 cycles at λ_1, 5 cycles at λ_2, 5 cycles at λ_3, 1 cycle at λ_1 due to failure) reached during the multiple uniaxial loading at the nominal tensile strain rate $1.s^{-1}$. Tangent modulus (MPa) is calculated as the derivative of the stress versus longitudinal strain. Voiding rate (in %) is calculated as the derivative of the DIC void fraction as a function of the longitudinal strain. Heat source is calculated by using equation 4. Filled symbols are for the 1st cycle and unfilled symbols for the 2nd to 5th cycles. For sake of clarity only the loadings are shown for the tangent modulus and voiding rate.

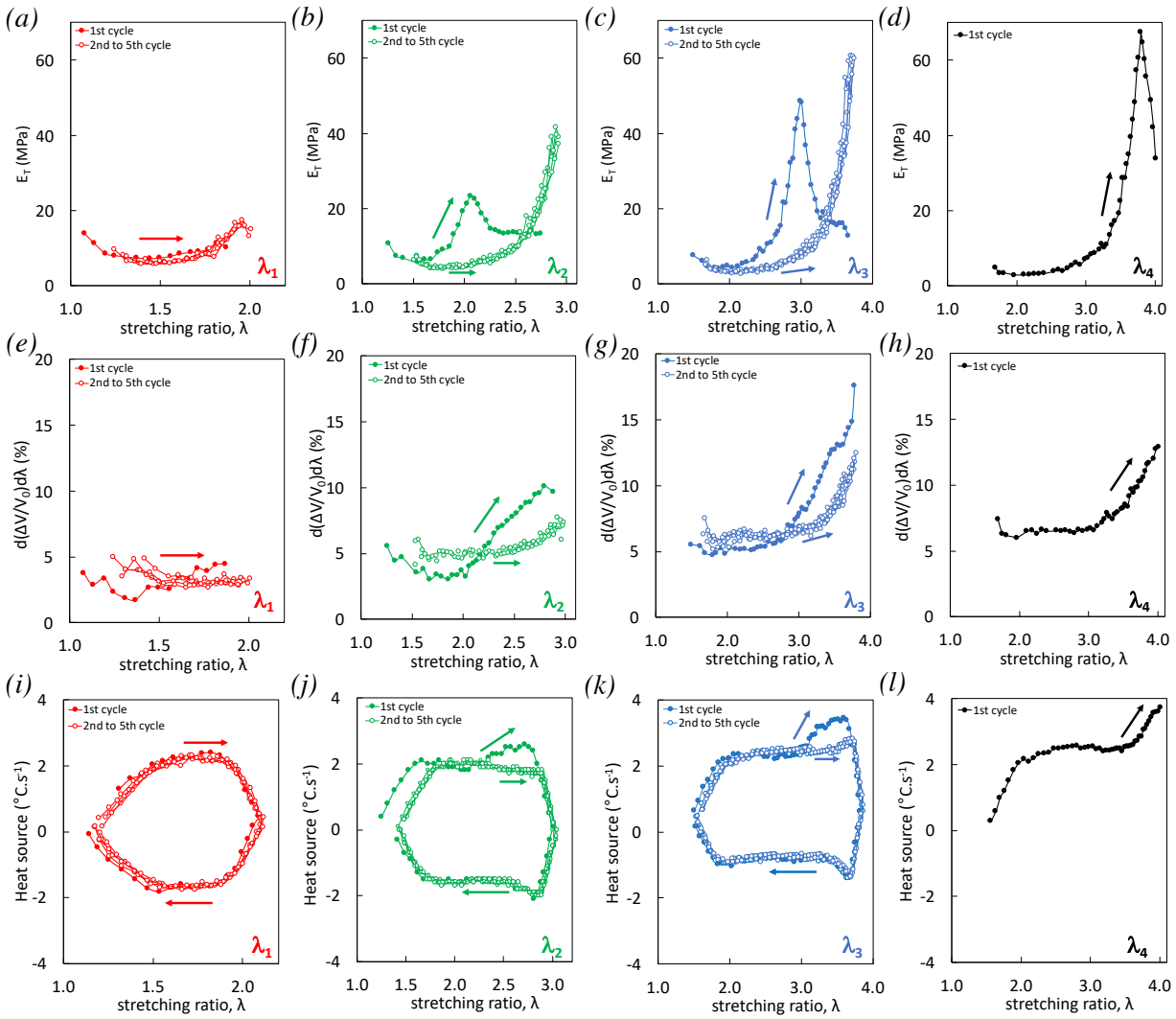

Figure 9. Tangent modulus *(a-d)*, voiding rate *(e-h)* and heat source *(i-l)* of EPDM-40 versus the different successive maximum strain (5 cycles at λ_1, 5 cycles at λ_2, 5 cycles at λ_3, 1 cycle at λ_1 due to failure) reached during the multiple uniaxial loading at the nominal tensile strain rate $1.s^{-1}$. Tangent modulus (MPa) is calculated as the derivative of the stress versus longitudinal strain. Voiding rate (in %) is calculated as the derivative of the DIC void fraction as a function of the longitudinal strain. Heat source is calculated by using equation 4. Filled symbols are for the 1st cycle and unfilled symbols for the 2nd to 5th cycles. For sake of clarity only the loadings are shown for the tangent modulus and voiding rate.

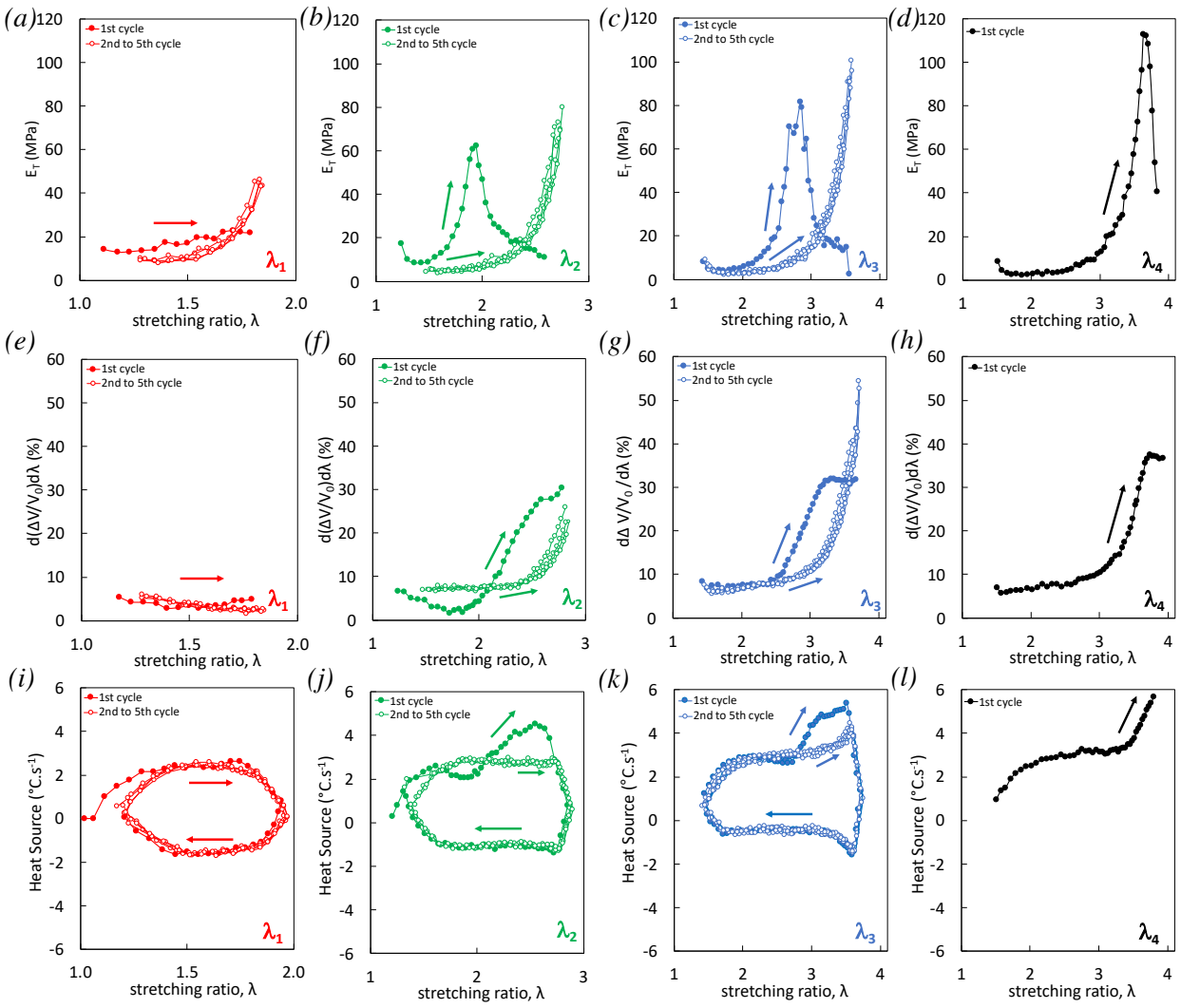

Figure 10. Tangent modulus *(a-d)*, voiding rate *(e-h)* and heat source *(i-l)* of EPDM-80 versus the different successive maximum strain (5 cycles at λ_1, 5 cycles at λ_2, 5 cycles at λ_3, 1 cycle at λ_1 due to failure) reached during the multiple uniaxial loading at the nominal tensile strain rate $1.s^{-1}$. Tangent modulus (MPa) is calculated as the derivative of the stress versus longitudinal strain. Voiding rate (in %) is calculated as the derivative of the DIC void fraction as a function of the longitudinal strain. Heat source is calculated by using equation 4. Filled symbols are for the 1st cycle and unfilled symbols for the 2nd to 5th cycles. For sake of clarity only the loadings are shown for the tangent modulus and voiding rate.

Finally, a comparison of the strain dependence of the tangent modulus, voiding rate and heat source, is performed. First, the strain at tangent modulus upturn nicely corresponds to the maximum strain reached at each series of cycle up to λ_2, λ_3 and λ_4 (**Figure 11a**) that hence seems

to be a good indicator of Mullins effect associated with the transition from a series of cycle to another with incremental strain. For the second series of cycles ($\lambda_{max}=\lambda_2 \approx 2$) voiding rate upturn (**Figure 11b**) and heart source upturn (**Figure 11c**) in filled EPDM both occur simultaneously with tangent modulus upturn. Hence, in this strain range, Mullins damage is associated with the acceleration of dissipative cavitation mechanisms – by nucleation of new cavities and/or increase of cavities growth – at the moment when strain surpasses λ_{max}. At higher strain, ($\lambda_{max}=\lambda_2$ and λ_3) the heat source upturn precedes the maximum tangent modulus. The heat source is in turn preceded by voiding rate upturn suggesting more complex molecular mechanisms to occur in this strain range, prior macroscopic breakage of rubber material. This may reflect our previous findings on the same series of filled EPDM suggesting damage mechanisms at large strain not only to involve chains rupture and/or debonding at rubber-filler interface typical for Mullins damage but also to release the occluded rubber [43].

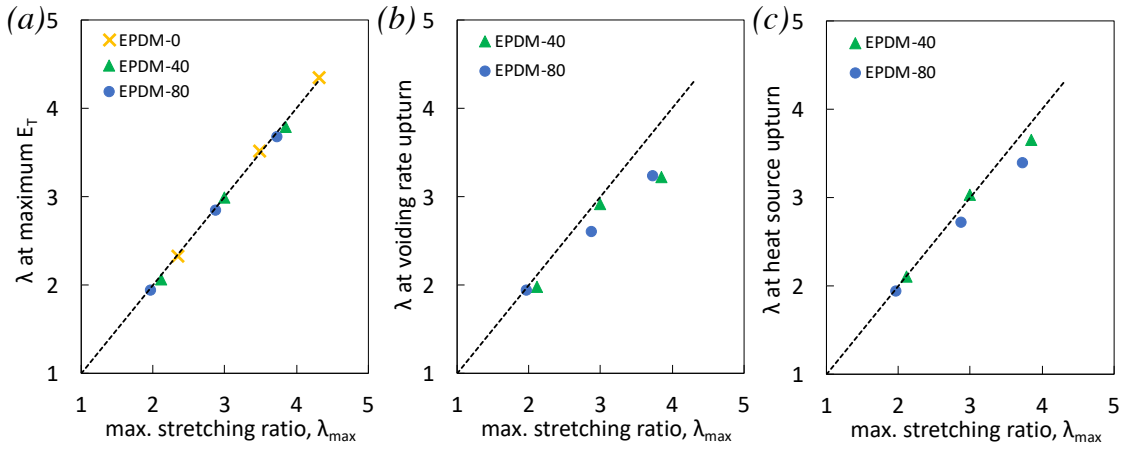

Figure 11. Maximum of tangent modulus *(a)*, upturn of voiding rate *(b)* and upturn of heat source *(c)* versus the maximum stretching ratio, respectively λ_1, λ_2, λ_3 and λ_4, for EPDM-0 (cross symbols), EPDM-40 (triangle symbols) and EPDM-80 (circle symbols) measured at the first loading of each cyclic series. In figure *(b)* and *(c)*, no signature of voiding rate upturn and heat source upturn for EPDM-0. The strain at upturns, λ_{upturn}, of heat source and voiding rate are calculated as the interception of two linear slopes that fit the experimental data in the strain range [λ_{upturn}-0.5, λ_{upturn}+0.5].

3. Conclusion

We have investigated the thermomechanical coupling of Mullins damage in filled EPDM. This has been carried out by tracking traces of self-heating on specimen surface measured by Infrared thermography (IR) combined with voiding fraction measured by Digital Image Correlation (DIC) during high strain rate cycles up to failure. We first identified that volumetric strain accompanying the rubber deformation is mostly due to strain induced damage, while thermal expansion caused by self-heating has a negligible contribution. The thermomechanical coupling associated with Mullins phenomenon has been identified by evaluating (i) tangent modulus, (ii) voiding rate and (iii) heat sources. The tangent modulus reaches a maximum at the strain transition, $\lambda_{max,}$ from a series of cycle to another (by incremental strain) and hence found to be an appropriate mechanical signature of Mullin effect. When the strain surpasses λ_{max}, both voiding rate upturn and heat source upturn are observed during the first loading of each series of cycles. These signatures suggest Mullins damage at high strain rate to be associated with the (re)-activation of dissipative cavitation mechanisms, by nucleation of new cavities and/or acceleration of cavities growth.

This study points out the question of how self-heating may intervene in certain industrial applications with high thermomechanical coupling. This is the case of mechanical devulcanization such as the high-shear mixing (HSM) [2], [50], [51] which is of significance for the recycling of waste rubbers. At moderate self-heating (below the vulcanization temperature), the efficiency of HSM process may be lowered by delayed voiding (due to lowered material viscosity) that in turn may prevent devulcanization. Additionally, an uncontrolled high self-heating above the vulcanization temperature may also prevent devulcanization by reactivating sulphur-vulcanization or even by favouring sulphur bond reversion. The fine tune of the loading conditions (deformation rate, number of cycles, incremental cycles) may hence help to optimize such processing.

Data availability

Data will be made available on request.

Declaration of competing interest

The authors declare that they have no known competing financial interests or personal relationships that could have appeared to influence the work reported in this paper.

CRediT authorship contribution statement

Nicolas Candau: Conceptualization, Data curation, Formal analysis, Investigation, original draft, review and editing. Oguzhan Oguz: Investigation, original draft, review and editing. Edith Peuvrel-Disdier: Funding acquisition, Investigation, Supervision, review and editing. Jean-Luc Bouvard: Funding acquisition, Investigation, Supervision, review and editing. Maria Lluisa Maspoch: Funding acquisition, Supervision, review and editing. Guillaume Corvec: Data curation, Formal analysis, review and editing. Christophe Pradille: Data curation, Investigation, Supervision, review and editing. Noelle Billon: Funding acquisition, Supervision, review and editing.

4. Acknowledgements

The authors gratefully acknowledge funding from the European Union's Horizon 2020 research and innovation programme under the Marie Skłodowska-Curie grant agreement No 712949 (TECNIOspring PLUS). The authors acknowledge the ECOTHER project supported by BPiFrance. The authors are indebted to the company SACRED for processing the rubber gum and to the laboratory GEPEA (University of Nantes) for the curing procedure of rubber compounds.

5. References

[1] S. L. Sokolov, « Prediction of the fatigue life of pneumatic tires », *J. Mach. Manuf. Reliab.*, vol. 39, n° 5, p. 459-465, 2010, doi: 10.3103/S1052618810050092.

[2] R. Diaz, G. Colomines, E. Peuvrel-Disdier, et R. Deterre, « Thermo-mechanical recycling of rubber: Relationship between material properties and specific mechanical energy », *J. Mater. Process. Technol.*, vol. 252, p. 454-468, 2018, doi: 10.1016/j.jmatprotec.2017.10.014.

[3] J. R. Samaca Martinez, J.-B. Le Cam, X. Balandraud, E. Toussaint, et J. Caillard, « New elements concerning the Mullins effect: A thermomechanical analysis », *Eur. Polym. J.*, vol. 55, p. 98-107, 2014, doi: 10.1016/j.eurpolymj.2014.03.014.

[4] P. A. Kakavas, « Mechanical properties of bonded elastomer discs subjected to triaxial stress », *J. Appl. Polym. Sci.*, vol. 59, n° 2, p. 251-261, 1996, doi: 10.1002/(SICI)1097-4628(19960110)59:2<251::AID-APP9>3.0.CO;2-W.

[5] M. Cheng et W. Chen, « Experimental investigation of the stress–stretch behavior of EPDM rubber with loading rate effects », *Int. J. Solids Struct.*, vol. 40, n° 18, p. 4749-4768, 2003, doi: 10.1016/S0020-7683(03)00182-3.

[6] D. E. Hanson *et al.*, « Stress softening experiments in silica-filled polydimethylsiloxane provide insight into a mechanism for the Mullins effect », *Polymer*, vol. 46, n° 24, p. 10989-10995, 2005, doi: 10.1016/j.polymer.2005.09.039.

[7] R. Diaz, J. Diani, et P. Gilormini, « Physical interpretation of the Mullins softening in a carbon-black filled SBR », *Polymer*, vol. 55, n° 19, p. 4942-4947, sept. 2014, doi: 10.1016/j.polymer.2014.08.020.

[8] H. J. Qi et M. C. Boyce, « Stress–strain behavior of thermoplastic polyurethanes », *Mech. Mater.*, vol. 37, n° 8, p. 817-839, 2005, doi: 10.1016/j.mechmat.2004.08.001.

[9] T. Sui *et al.*, « Strain softening of nano-scale fuzzy interfaces causes Mullins effect in thermoplastic polyurethane », *Sci. Rep.*, vol. 7, nº 1, Art. nº 1, 2017, doi: 10.1038/s41598-017-00904-3.

[10] H. Yuk, T. Zhang, G. A. Parada, X. Liu, et X. Zhao, « Skin-inspired hydrogel–elastomer hybrids with robust interfaces and functional microstructures », *Nat. Commun.*, vol. 7, nº 1, Art. nº 1, 2016, doi: 10.1038/ncomms12028.

[11] R. E. Webber, C. Creton, H. R. Brown, et J. P. Gong, « Large Strain Hysteresis and Mullins Effect of Tough Double-Network Hydrogels », *Macromolecules*, vol. 40, nº 8, p. 2919-2927, 2007, doi: 10.1021/ma062924y.

[12] E. Peña et M. Doblaré, « An anisotropic pseudo-elastic approach for modelling Mullins effect in fibrous biological materials », *Mech. Res. Commun.*, vol. 36, nº 7, p. 784-790, oct. 2009, doi: 10.1016/j.mechrescom.2009.05.006.

[13] J.-B. Le Cam, « A REVIEW OF VOLUME CHANGES IN RUBBERS: THE EFFECT OF STRETCHING », *Rubber Chem. Technol.*, vol. 83, nº 3, p. 247-269, 2010, doi: 10.5254/1.3525684.

[14] J.-M. Chenal, C. Gauthier, L. Chazeau, L. Guy, et Y. Bomal, « Parameters governing strain induced crystallization in filled natural rubber », *Polymer*, vol. 48, nº 23, p. 6893-6901, 2007, doi: 10.1016/j.polymer.2007.09.023.

[15] Y. Merckel, J. Diani, M. Brieu, et J. Caillard, « Effects of the amount of fillers and of the crosslink density on the mechanical behavior of carbon-black filled styrene butadiene rubbers », *J. Appl. Polym. Sci.*, vol. 129, nº 4, p. 2086-2091, 2013, doi: 10.1002/app.38925.

[16] N. Candau, « Compréhension des mécanismes de cristallisation sous tension des élastomères en conditions quasi-statiques et dynamiques », Doctoral Thesis, Lyon, INSA, 2014.

[17] N. Candau, L. Chazeau, J.-M. Chenal, C. Gauthier, et E. Munch, « Complex dependence on the elastically active chains density of the strain induced crystallization of vulcanized natural rubbers, from low to high strain rate », *Polymer*, vol. 97, p. 158-166, 2016, doi: 10.1016/j.polymer.2016.05.020.

[18] A. De Almeida, L. Chazeau, G. Vigier, G. Marque, et Y. Goutille, « Influence of PE/PP ratio and ENB content on the degradation kinetics of γ-irradiated EPDM », *Polym. Degrad. Stab.*, vol. 110, p. 175-183, 2014, doi: 10.1016/j.polymdegradstab.2014.08.029.

[19] F. Grasland, L. Chazeau, J.-M. Chenal, et R. schach, « About thermo-oxidative ageing at moderate temperature of conventionally vulcanized natural rubber », *Polym. Degrad. Stab.*, vol. 161, p. 74-84, 2019, doi: 10.1016/j.polymdegradstab.2018.12.029.

[20] R. Diaz, G. Colomines, E. Peuvrel-Disdier, et R. Deterre, « Thermo-mechanical recycling of rubber: Relationship between material properties and specific mechanical energy », *J. Mater. Process. Technol.*, vol. 252, p. 454-468, 2018, doi: 10.1016/j.jmatprotec.2017.10.014.

[21] N. Candau, O. Oguz, E. Peuvrel-Disdier, J.-L. Bouvard, C. Pradille, et N. Billon, « Strain-induced network chains damage in carbon black filled EPDM », *Polymer*, vol. 175, p. 329-338, 2019, doi: 10.1016/j.polymer.2019.05.017.

[22] N. Candau, J.-L. Bouvard, E. Peuvrel-Disdier, R. Valette, et N. Billon, « Effect of stretching on the network structure of carbon black filled EPDM rubbers. » 16th Elastomery Conference (Elastomery 2015). 2015, Tour (France). 2p. hal-01502249.

[23] H. Zhang *et al.*, « Nanocavitation in Carbon Black Filled Styrene–Butadiene Rubber under Tension Detected by Real Time Small Angle X-ray Scattering », *Macromolecules*, vol. 45, nº 3, p. 1529-1543, 2012, doi: 10.1021/ma2023606.

[24] D. Rittel, « On the conversion of plastic work to heat during high strain rate deformation of glassy polymers », *Mech. Mater.*, vol. 31, n° 2, p. 131-139, 1999, doi: 10.1016/S0167-6636(98)00063-5.

[25] P. Duchene, S. Chaki, A. Ayadi, et P. Krawczak, « A review of non-destructive techniques used for mechanical damage assessment in polymer composites », *J. Mater. Sci.*, vol. 53, n° 11, p. 7915-7938, 2018, doi: 10.1007/s10853-018-2045-6.

[26] C. Colombo, L. Vergani, et M. Burman, « Static and fatigue characterisation of new basalt fibre reinforced composites », *Compos. Struct.*, vol. 94, n° 3, p. 1165-1174, 2012, doi: 10.1016/j.compstruct.2011.10.007.

[27] G. La Rosa et A. Risitano, « Thermographic methodology for rapid determination of the fatigue limit of materials and mechanical components », *Int. J. Fatigue*, vol. 22, n° 1, p. 65-73, 2000, doi: 10.1016/S0142-1123(99)00088-2.

[28] N. Candau, L. Chazeau, J.-M. Chenal, C. Gauthier, et E. Munch, « Compared abilities of filled and unfilled natural rubbers to crystallize in a large strain rate domain », *Compos. Sci. Technol.*, vol. 108, p. 9-15, 2015, doi: 10.1016/j.compscitech.2014.12.014.

[29] J. Montesano, Z. Fawaz, et H. Bougherara, « Use of infrared thermography to investigate the fatigue behavior of a carbon fiber reinforced polymer composite », *Compos. Struct.*, vol. 97, p. 76-83, 2013, doi: 10.1016/j.compstruct.2012.09.046.

[30] J. R. Samaca Martinez, J.-B. Le Cam, X. Balandraud, E. Toussaint, et J. Caillard, « Filler effects on the thermomechanical response of stretched rubbers », *Polym. Test.*, vol. 32, n° 5, p. 835-841, 2013, doi: 10.1016/j.polymertesting.2013.04.003.

[31] J.-B. Le Cam, J. R. Samaca Martinez, X. Balandraud, E. Toussaint, et J. Caillard, « Thermomechanical Analysis of the Singular Behavior of Rubber: Entropic Elasticity,

Reinforcement by Fillers, Strain-Induced Crystallization and the Mullins Effect », *Exp. Mech.*, vol. 55, n° 4, p. 771-782, 2015, doi: 10.1007/s11340-014-9908-9.

[32] A. Chrysochoos, V. Huon, F. Jourdan, J.-M. Muracciole, R. Peyroux, et B. Wattrisse, « Use of Full-Field Digital Image Correlation and Infrared Thermography Measurements for the Thermomechanical Analysis of Material Behaviour », *Strain*, vol. 46, n° 1, p. 117-130, 2010, doi: 10.1111/j.1475-1305.2009.00635.x.

[33] A. Maurel-Pantel, E. Baquet, J. Bikard, J. L. Bouvard, et N. Billon, « A thermo-mechanical large deformation constitutive model for polymers based on material network description: Application to a semi-crystalline polyamide 66 », *Int. J. Plast.*, vol. 67, p. 102-126, 2015, doi: 10.1016/j.ijplas.2014.10.004.

[34] J. R. Samaca Martinez, X. Balandraud, E. Toussaint, J.-B. Le Cam, et D. Berghezan, « Thermomechanical analysis of the crack tip zone in stretched crystallizable natural rubber by using infrared thermography and digital image correlation », *Polymer*, vol. 55, n° 24, p. 6345-6353, nov. 2014, doi: 10.1016/j.polymer.2014.10.010.

[35] N. Candau, C. Pradille, J.-L. Bouvard, et N. Billon, « On the use of a four-cameras stereovision system to characterize large 3D deformation in elastomers », *Polym. Test.*, vol. 56, p. 314-320, 2016, doi: 10.1016/j.polymertesting.2016.10.017.

[36] N. Candau, J.-L. Bouvard, E. Peuvrel-Disdier, R. Valette, C. Pradille, et N. Billon, « Coupled thermal and volume change measurements during stretching of filled EPDM rubbers », 10th International Conference on Mechanics of Time-Dependent Materials (MTDM2016), 2016, hal-01499444.

[37] A. Benaarbia, A. Chrysochoos, et G. Robert, « Kinetics of stored and dissipated energies associated with cyclic loadings of dry polyamide 6.6 specimens », *Polym. Test.*, vol. 34, p. 155-167, 2014, doi: 10.1016/j.polymertesting.2014.01.009.

[38] J. R. Samaca Martinez, J.-B. Le Cam, X. Balandraud, E. Toussaint, et J. Caillard, « Mechanisms of deformation in crystallizable natural rubber. Part 2: Quantitative calorimetric analysis », *Polymer*, vol. 54, n° 11, p. 2727-2736, 2013, doi: 10.1016/j.polymer.2013.03.012.

[39] W. Harizi, S. Chaki, G. Bourse, et M. Ourak, « Mechanical damage assessment of Polymer–Matrix Composites using active infrared thermography », *Compos. Part B Eng.*, vol. 66, p. 204-209, 2014, doi: 10.1016/j.compositesb.2014.05.017.

[40] Y. Y. Hung *et al.*, « Review and comparison of shearography and active thermography for nondestructive evaluation », *Mater. Sci. Eng. R Rep.*, vol. 64, n° 5, p. 73-112, 2009, doi: 10.1016/j.mser.2008.11.001.

[41] G. Kraus et J. T. Gruver, « Thermal expansion, free volume, and molecular mobility in a carbon black-filled elastomer », *J. Polym. Sci. Part -2 Polym. Phys.*, vol. 8, n° 4, p. 571-581, 1970, doi: 10.1002/pol.1970.160080408.

[42] C. W. V. D. Wal, H. W. Bree, et F. R. Schwarzl, « Mechanical properties of highly filled elastomers. II. Relationship between filler characteristics, thermal expansion, and bulk moduli », *J. Appl. Polym. Sci.*, vol. 9, n° 6, p. 2143-2166, 1965, doi: 10.1002/app.1965.070090611.

[43] N. Candau, O. Oguz, E. Peuvrel-Disdier, J.-L. Bouvard, C. Pradille, et N. Billon, « Strain and filler ratio transitions from chains network to filler network damage in EPDM during single and cyclic loadings », *Polymer*, vol. 197, p. 122435, 2020, doi: 10.1016/j.polymer.2020.122435.

[44] K. Yamaguchi, J. J. C. Busfield, et A. G. Thomas, « Electrical and mechanical behavior of filled elastomers. I. The effect of strain », *J. Polym. Sci. Part B Polym. Phys.*, vol. 41, nº 17, p. 2079-2089, 2003, doi: 10.1002/polb.10571.

[45] L. Mullins, « Softening of Rubber by Deformation », *Rubber Chem. Technol.*, vol. 42, nº 1, p. 339-362, 1969, doi: 10.5254/1.3539210.

[46] J. a. C. Harwood, L. Mullins, et A. R. Payne, « Stress softening in natural rubber vulcanizates. Part II. Stress softening effects in pure gum and filler loaded rubbers », *J. Appl. Polym. Sci.*, vol. 9, nº 9, p. 3011-3021, 1965, doi: 10.1002/app.1965.070090907.

[47] G. R. Hamed, « Molecular Aspects of the Fatigue and Fracture of Rubber », *Rubber Chem. Technol.*, vol. 67, nº 3, p. 529-536, 1994, doi: 10.5254/1.3538689.

[48] J. K. Cho *et al.*, « Heat dissipative mechanical damping properties of EPDM rubber composites including hybrid fillers of aluminium nitride and boron nitride », *Soft Matter*, vol. 16, nº 29, p. 6812-6818, 2020, doi: 10.1039/C9SM02123J.

[49] Q. Demassieux, D. Berghezan, S. Cantournet, H. Proudhon, et C. Creton, « Temperature and aging dependence of strain-induced crystallization and cavitation in highly crosslinked and filled natural rubber », *J. Polym. Sci. Part B Polym. Phys.*, vol. 57, nº 12, p. 780-793, 2019, doi: 10.1002/polb.24832.

[50] O. Oguz *et al.*, « High-Performance Green Composites of Poly(lactic acid) and Waste Cellulose Fibers Prepared by High-Shear Thermokinetic Mixing », *Ind. Eng. Chem. Res.*, vol. 56, nº 30, p. 8568-8579, 2017, doi: 10.1021/acs.iecr.7b02037.

[51] O. Oguz, N. Candau, M. K. Citak, F. N. Cetin, S. Avaz Seven, et Y. Z. Menceloglu, « A Sustainable Approach to Produce Stiff, Super-Tough, and Heat-Resistant Poly(lactic acid)-

Based Green Materials », *ACS Sustain. Chem. Eng.*, vol. 7, n° 8, p. 7869-7877, 2019, doi: 10.1021/acssuschemeng.9b00319.